A FUNDAMENTAL STUDY ON STRUCTURAL PERFORMANCE OF *CES* SHEAR WALLS WITH DIFFERENT ANCHORAGE CONDITION OF WALL REINFORCING BARS

Suguru SUZUKI
JSPS Research Fellow, Dept. of Architectural Eng., Osaka University, Suita, Japan

Tomoya MATSUI
Assistant Prof., Dept. of Architecture and Civil Eng., Toyohashi Univ. of Technology, Toyohashi, Japan

Hiroshi KURAMOTO
Prof., Dept. of Architectural Eng., Osaka University, Suita, Japan

SUMMARY:
This paper describes the structural performance of CES shear walls obtained from cyclic loading tests. The experimental variables were the shear-span ratio and anchorage condition of the longitudinal wall reinforcement. The results show that the effect of the anchorage conditions of longitudinal wall reinforcing bars on both the shear and flexural strength of CES shear walls are not significant. The deformation capacity of the CES shear walls is slightly improved by omitting the wall's longitudinal reinforcement anchorage, because the damaged area of FRC in the wall panel is reduced by increasing in the horizontal slip between the wall panel and boundary beams.

Keywords: CES Shear Walls, Cyclic Loading Test, Anchorage Condition, Fiber Reinforced Concrete, Shear span ratio

1. INTRODUCTION

The steel reinforced concrete (SRC) structures show good structural performance in terms of resisting lateral forces imposed by earthquakes. It has been widely used for medium-rise, high-rise, and super high-rise buildings in Japan. However, since the 1990s, the number of SRC buildings constructed has decreased. Although this decrease might be because of the development of new structural building systems such as the high-strength concrete structure or concrete-filled steel tube structure, the main reason seems to be the construction problems of SRC structures, like the construction costs and longer construction schedules compared with other conventional structural systems. Even so, it could be important that SRC structures provide the similar or better seismic performance than other structural systems. Therefore, the authors aim to develop a new structural system with a seismic performance as good as SRC structures, along with good workability, and have conducted a continuing development study on Composite Concrete Encased Steel (CES) structures composed of steel and fiber reinforced concrete (FRC). In experimental studies on CES columns, CES beam-column joints, and a two-bay two-story CES frame, it was confirmed that the CES structural system showed good and stable hysteresis characteristics (Kuramoto et al. 2007, Matsui et al. 2009).

On the other hand, the shear wall for the major seismic member is effective to increase the strength and stiffness of the CES structural system. However, it will be difficult to arrange wall reinforcing bars in the CES shear walls. Recently, there have been some researches on methods of jointing a frame and wall panel in SRC shear walls (Haruyama et al. 2006). It is likewise an important problem to improve the workability of a CES frame and FRC wall panel joint in the CES structure.

In this study, cyclic loading tests were carried out on CES shear walls with different anchorage method for connecting the FRC wall panel to the CES frame. The basic structural performance, such as ultimate strength, deformation capacity and failure modes, of the CES shear walls were investigated.

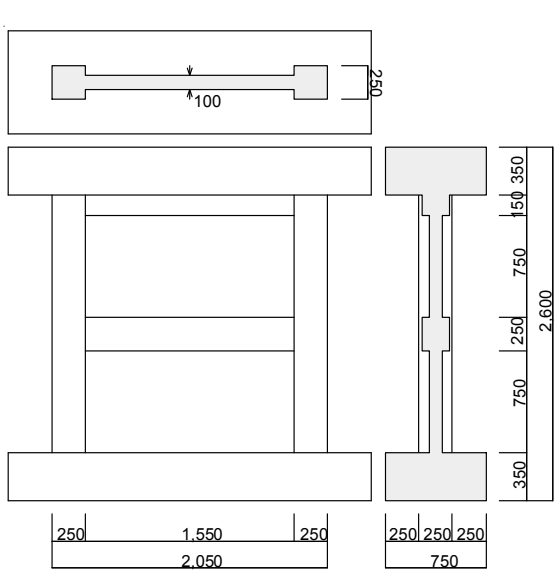

Figure 2.1 Test specimen

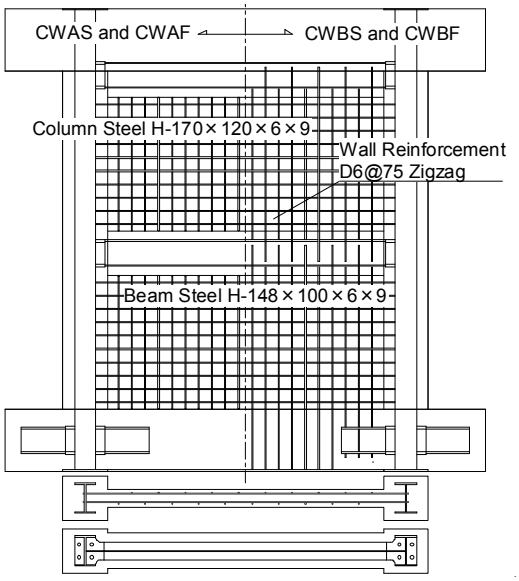

Figure 2.2 Bar arrangement

Table 2.1 Details of specimens

Specimens		*CWAS*	*CWAF*	*CWBS*	*CWBF*
Column	*B*x*D*	250x250 (mm)			
	Steel	H-170x120x6x9 ($_sp$=4.9%)			
Beam	*B*x*D*	200x250 (mm)			
	Steel	H-148x100x6x9 ($_gp$=5.2%)			
Wall	Thickness	100 (mm)			
	Longitudinal bar	D6@75 zigzag ($_wp$=0.42%)			
	Transverse bar				
Shear span ratio		1.1	1.65	1.1	1.65
Anchorage condition of longitudinal wall reinforcing bars		nonexistent		180° hook in beam	

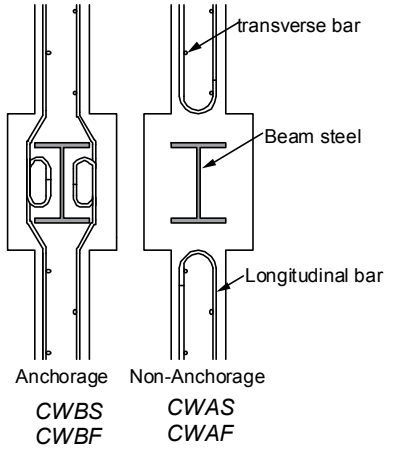

Figure 2.3 Bar arrangement in beam

2. TEST PROGRAM

2.1 Description of Specimens

The specimens were designed to simulate the lower two stories of a multi-story shear wall in a medium rise building, and were one-third-scale of prototype walls. Four specimens were prepared for this test.

The configurations and bar arrangements of the specimens are shown in Figs. 2.1, 2.2 and 2.3. Details of the sections are shown in Table 2.1. The column had a 250mm square cross-section, and the beam section was 200 mm x 250 mm. The column span length was 1,800 mm, and the wall thickness was 100 mm. The experimental variables were the shear-span ratio and anchorage condition of the longitudinal wall reinforcement. The shear-span ratio was 1.1 in Specimens CWAS and CWBS, and it was 1.65 in Specimens CWAF and CWBF. Specimens CWAS and CWBS were expected to be shear failure mode. Specimens CWAF and CWBF were expected to be flexural failure mode. The longitudinal wall reinforcing bars for Specimens CWAS and CWAF were bent in wall panel. On the other hand, the longitudinal reinforcing bars for Specimens CWBS and CWBF were anchored to a beam or stubs, as shown in Fig. 2.3. The transverse wall reinforcing bars in all specimens were securely fixed by welding them to the steel web in the CES boundary columns. In addition, the H-section steels of the boundary columns were anchored to the upper and lower stabs in all specimens.

The mechanical properties of the FRC and steel used are shown in Tables 2.2 and 2.3, respectively. Poly vinyl alcohol (PVA) fibers with a diameter of 0.66 mm and a length of 30 mm were used for the

Table 2.2 Mechanical properties of FRC

Specimen		σ_B (MPa)	E_C (GPa)	ε_{c0} (μ)	*Age* (day)
CWAS	1 story	38.6	24.8	2814	91
	2 story	36.4	26.7	2550	86
CWBS	1 story	42.0	25.7	2587	94
	2 story	30.6	29.5	2558	89
CWAF	1 story	41.2	25.5	2457	100
	2 story	38.6	27.6	2423	95
CWBF	1 story	40.1	24.9	2765	105
	2 story	35.9	24.8	3160	100

σ_B: Compressive strength, E_C: Elastic modulus,
ε_{c0}: Strain at compressive strength

Table 2.3 Mechanical properties of steel

	σ_y (MPa)	E_s (GPa)	σ_u (MPa)
PL-6 (SS400)	260	190	409
PL-9 (SS400)	282	197	418
D6 (SD295A)	345	190	501

σ_y: Yield strength, E_s: Elastic modulus,
σ_u: Tensile strength

FRC. The volumetric ratio of the fibers was 1.0 %.

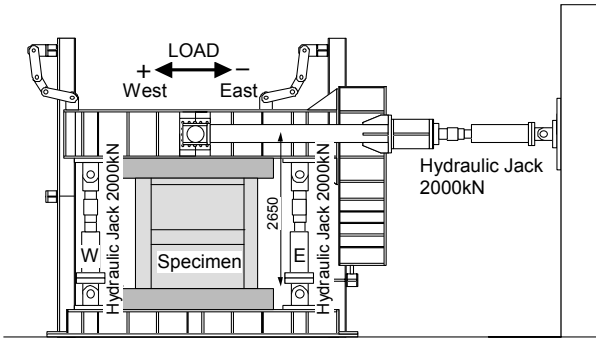

Figure 2.4 Loading apparatus

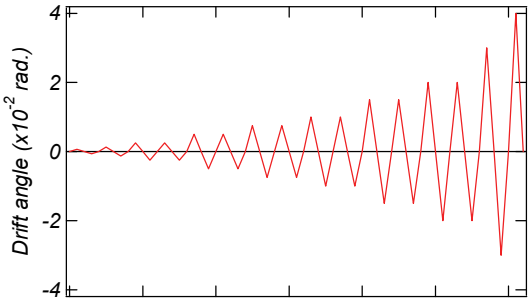

Figure 2.5 Loading cycle

2.2 Loading Program

The loading apparatus used is shown in Fig. 2.4. The wall specimens were loaded with horizontal cyclic shear forces using a hydraulic jack with a 2,000 kN capacity, while applying a constant axial force of 1,260 kN (N/N_0=0.2, where N=axial load, N_0=axial load capacity including steel of boundary columns) using two vertical manual jacks, each of which had a 2,000 kN capacity. During the testing, additional moment was also applied to the top of the specimen using the two vertical jacks to maintain the prescribed shear-span ratio of 1.1 or 1.65, using the following equations.

$$N_e = \frac{N_c}{2} - \frac{Q}{l}(h-a) \tag{2.1}$$

$$N_w = \frac{N_c}{2} + \frac{Q}{l}(h-a) \tag{2.2}$$

Where, N_e: axial force of east side jack, N_w: axial force of west side jack, N_c: constant axial force (1,260 kN), Q: shear force, l: distance between vertical jack, h: assumed height of applied shear force, and a: actual height of applied shear force.

The loading was conducted by controlling the relative drift angle, R, given by the ratio of the height corresponding to the measuring point for the horizontal displacement at the top of the specimen, h_0 (2,050 mm), to the horizontal deformation, δ, i.e., $R=\delta/h_0$. The horizontal load sequences consisted of one cycle for R of 0.0625 x 10^{-2} rad. and 0.125 x 10^{-2} rad. respectively, and after this from R of 0.25 x 10^{-2} rad. two cycles for each relative drift angle were applied as shown in Fig. 2.5.

3. EXPERIMENTAL RESULTS

3.1 Hysteresis Characteristics and Failure Modes

Shear force versus drift angle relationships of all specimens are shown in Fig. 3.1. Cracking patterns of all specimens are shown in Fig. 3.2 after loading cycles of 0.75 x 10^{-2} rad. and 3.0 x 10^{-2} rad.

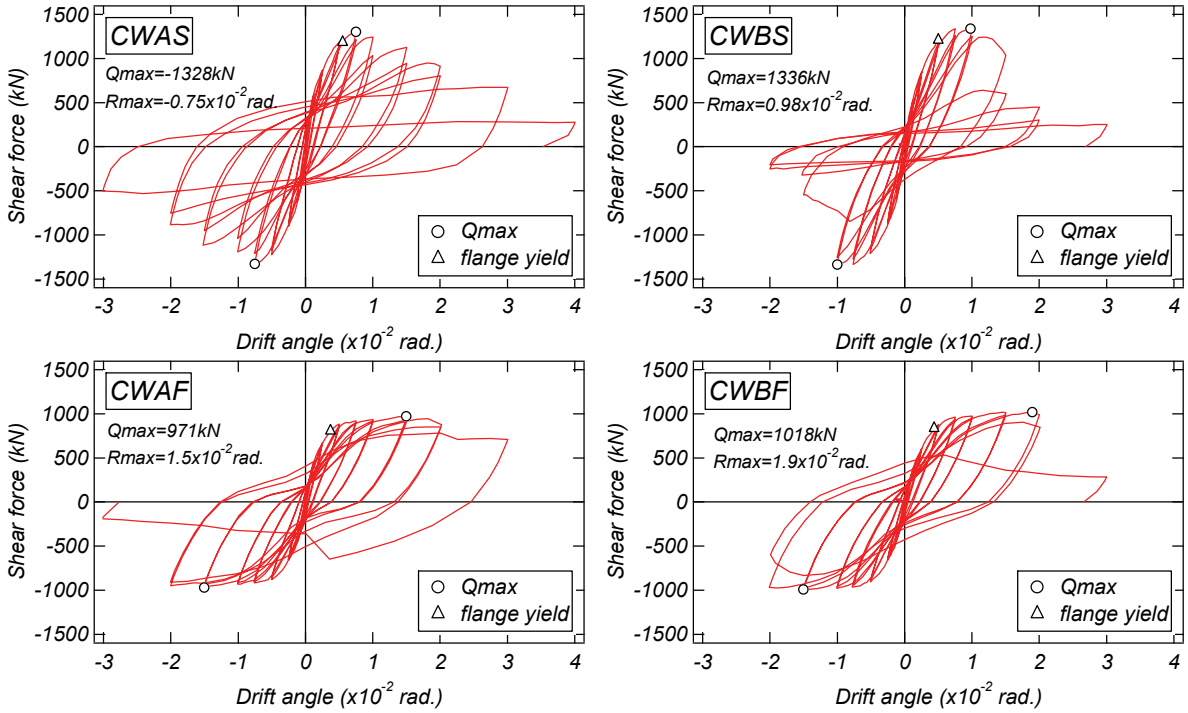

Figure 3.1 Shear force versus drift angle relationships

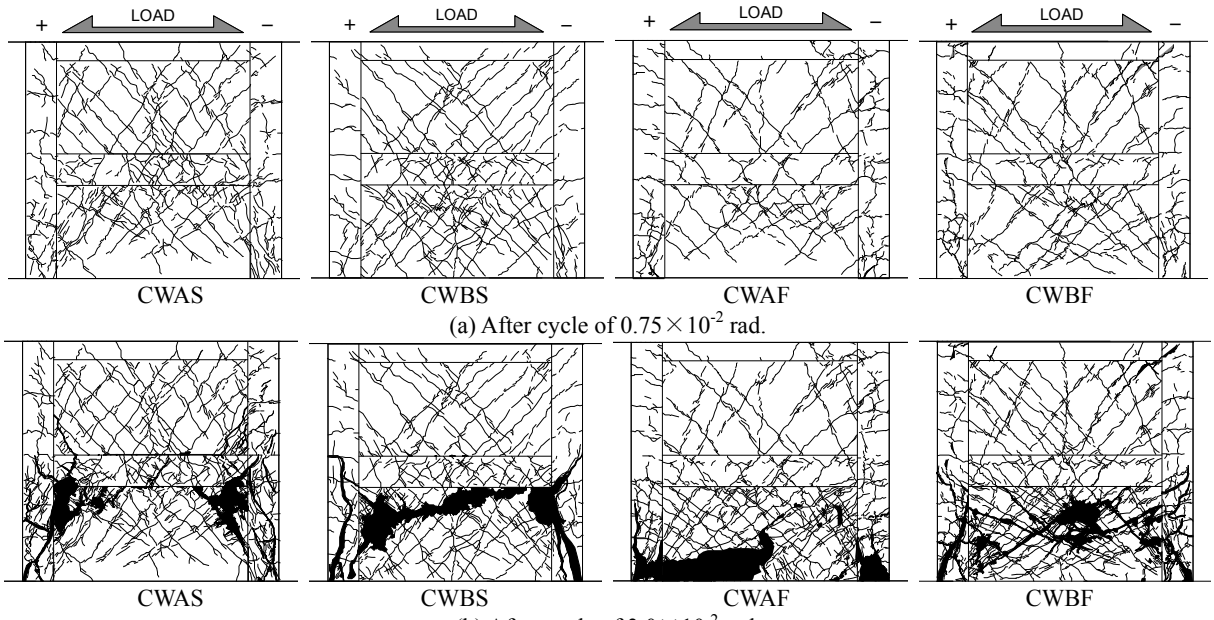

(a) After cycle of 0.75×10^{-2} rad.

(b) After cycle of 3.0×10^{-2} rad.

Figure 3.2 Cracking patterns

In Specimen CWAS, without longitudinal wall reinforcement anchorage, the maximum shear force reached -1,328 kN at R of -0.75 x 10^{-2} rad. In Specimen CWBS, with longitudinal wall reinforcement anchorage, the maximum shear force reached 1,336 kN at R of 0.98 x 10^{-2} rad. The maximum shear forces of these specimens were almost the same. However, the deformation capacity of Specimen CWAS and CWBS were different after reaching the maximum shear force. While the shear force of Specimen CWAS decreased slowly, that of Specimen CWBS decreased drastically at R of 1.5 x 10^{-2} rad.

Horizontal displacement between wall panel and beam versus drift angle relationships of all specimens

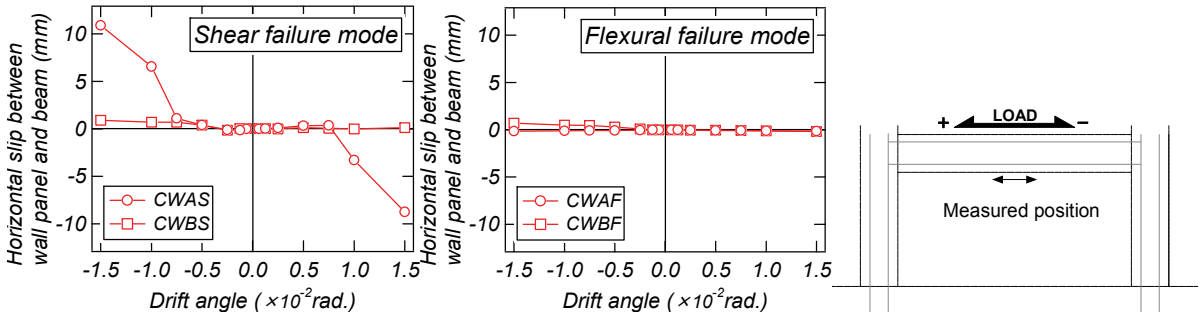

Figure 3.3 Horizontal slip between wall panel and beam

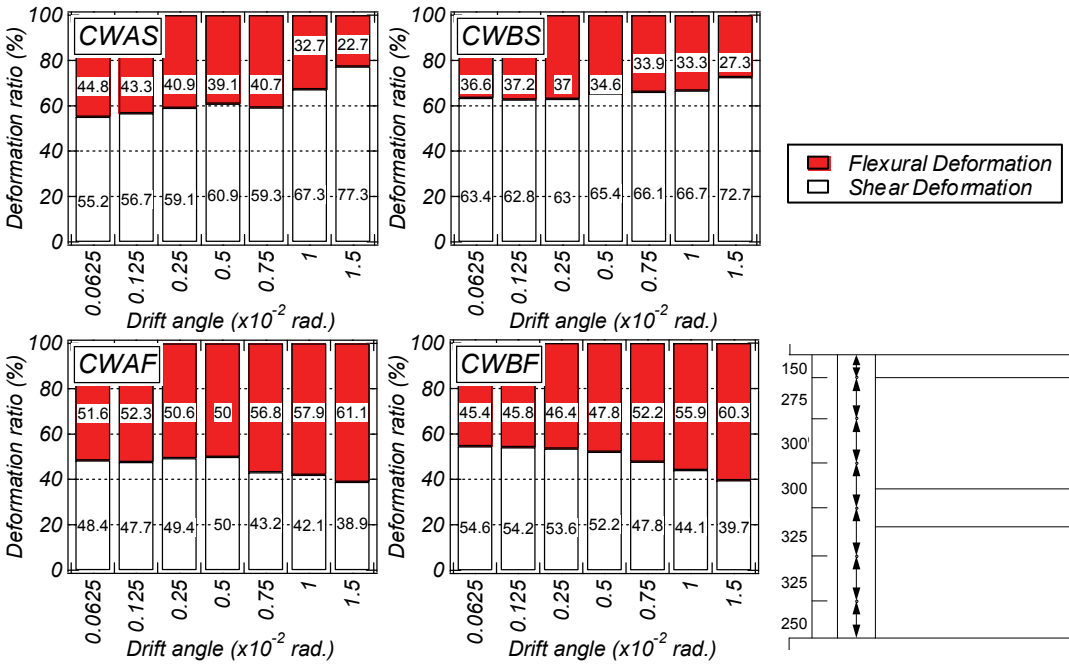

Figure 3.4 Deformation components

Figure 3.5 Measured positions

are shown in Fig. 3.3. In Specimens CWBS, with longitudinal wall reinforcement anchorage, the horizontal displacement between wall panel and beam hardly occurred. However, in Specimen CWAS, without longitudinal wall reinforcement anchorage, the horizontal slip between wall panel and beam increased at R of 1.0 x 10^{-2} rad. Therefore, it is thought that the observed difference of deformation capacity between Specimens CWAS and CWBS is because the damaged area of wall panel in Specimen CWAS was reduced by the occurrence of slip between the wall and boundary beam due to the absence of longitudinal wall reinforcement anchorage.

In Specimen CWAF, without longitudinal reinforcement anchorage, the maximum shear force reached 971 kN at R of 1.5 x 10^{-2} rad. In Specimen CWBF, with wall reinforcement anchorage, the maximum shear force reached 1,018 kN at R of 1.9 x 10^{-2} rad. The maximum shear forces of the two specimens are almost the same. Just after reaching R of 3.0 x 10^{-2} rad., Specimen CWAF showed significant strength deterioration in the negative loading, while the Specimen CWBF showed significant strength deterioration in the positive loading as shown in Fig. 3.1. It is found that the deformation capacity of Specimen CWBF was slightly poorer than that of Specimen CWAF.

Thus, it is found that the anchorage condition for the longitudinal reinforcement had little effect on the maximum shear force of the CES shear walls. In addition, the deformation capacity of the CES shear walls can be improved by omitting the anchorage of the longitudinal wall reinforcement.

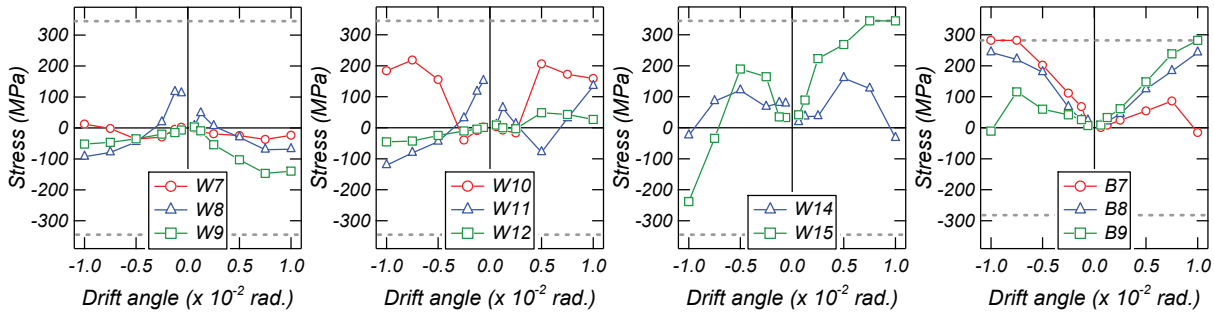

(a) CWAS

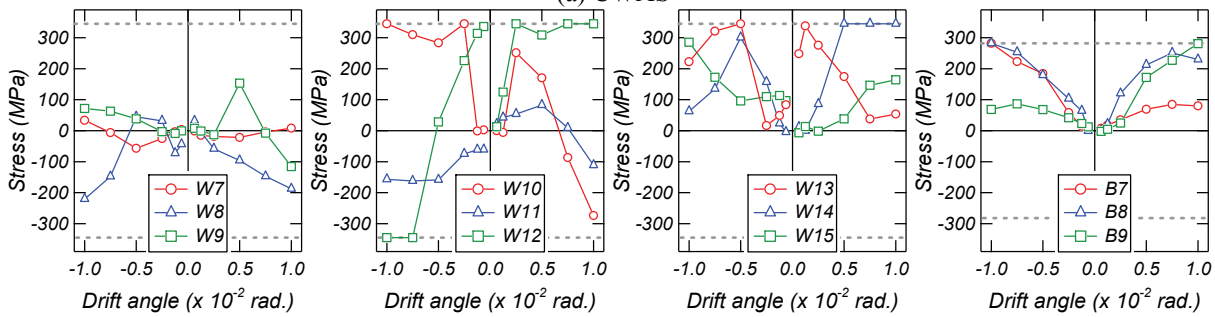

(b) CWBS

Figure 3.6 Stresses of the transverse wall reinforcing bars and steel flanges of the beams (Dashed line is yield stress)

3.2 Deformation Components

Figure 3.4 shows the contribution of shear deformation and flexural deformation to the total deformation of the all specimens until R of 1.5 x 10^{-2} rad. Flexural deformation was calculated using the axial displacement of boundary columns, as shown in Fig. 3.5, while shear deformation was calculated by subtracting the flexural deformation from the total deformation.

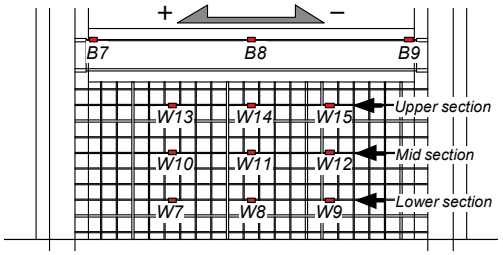

Figure 3.7 Measured position

The results for Specimens CWAS and CWBS which had the shear failure mode showed that the shear deformation was larger than the flexural deformation until R of 1.5 x 10^{-2} rad. While the results for Specimens CWAF and CWBF which had the flexural failure mode showed that the shear deformation and the flexural deformation were almost the same at R of 0.0625 x 10^{-2} rad. However the flexural deformation ratio increased with the increase of drift angle in Specimens CWAF and CWBF. The flexural deformations in Specimens CWAS and CWAF were larger than those in Specimens CWBS and CWBF, because the longitudinal reinforcing bars were anchored in Specimens CWBS and CWBF.

3.3 Transition of Stresses in Wall Transverse Reinforcing Bars and Beam Steel

Figure 3.6 shows the stresses of the transverse wall reinforcing bars and steel flange of the beam in Specimens CWAS and CWBS, which exhibited shear failure. The stresses were calculated using the measured strain and the bilinear hysteresis assumption for the steel. The strains were measured at the lower section, the mid section, the upper section of the wall panel, and the upper flange of the beam, as shown Fig. 3.7.

In Specimen CWAS, the transverse reinforcement at the position W15 of the wall panel yielded at R of 0.75 x 10^{-2} rad. In Specimen CWBS, the transverse reinforcements at the position W10, W12, W13 and W14 of the wall panel yielded until R of 0.75 x 10^{-2} rad. However the stresses on the wall reinforcement at lower section did not yield in both specimens. These situations are corresponding with the observed damage of the concrete wall panel shown Fig. 3.2.

As for steel in the beam, the stresses increased with increase of drift angle in both specimens. In addition, the upper flange in the beam was near to the yielding at R of 0.75 x 10^{-2} rad. in both specimens. It was confirmed that the steel in the beam effectively resisted the shear force.

4. EVALUATION OF ULTIMATE STRENGTH

The calculation results of the ultimate strengths for all specimens are listed in Table 4.1. The flexural strength was calculated using Eqn. 4.1, which is omitting the term of the reinforcing bars in the boundary column from an equation given in the "AIJ Standards for Structural Calculation of Steel Reinforced Concrete Structures". Moreover, the wall longitudinal reinforcing bars were not considered in the calculation for Specimens CWAS and CWAF, without wall reinforcement anchorage.

The shear strength was calculated using the Truss-Arch Equation (Eqn. 4.2). It is assumed that the flexural capacity of the boundary column contribute to the shear strength of the CES shear walls, as expressed, M_u, Eqn. 4.3. The shear strength was calculated by adding the lower steel flange of the beam to the transverse wall reinforcement, because it was observed that the steel flange of the beam yielded at the maximum strength of the wall, as shown in Eqn. 4.5.

Flexural strength equation

$$Q_{mu} = \left(\frac{N_U}{2} + {}_{sCS}A \cdot {}_s\sigma_y \cdot + \frac{{}_{mW}A}{2} {}_W\sigma_y\right) l_w / h_w \tag{4.1}$$

Shear strength by Truss-Arch equation

$$Q_{su} = {}_W t \left\{ {}_W l_t \cdot p_{se} \cdot {}_W\sigma_Y \cot\phi + \tan\theta(1-\beta) {}_W l_a \cdot \nu \cdot \frac{{}_c\sigma_B}{2} \right\} \tag{4.2}$$

$${}_W l_a = l' + D + \frac{1}{\cos\theta} \sqrt{\frac{2_{CS} M_U}{\nu \cdot \sigma_B \cdot {}_W t(1-\beta)}} \tag{4.3}$$

$$\beta = \frac{2 p_{se} \cdot {}_W\sigma_Y}{\nu \cdot {}_c\sigma_B} \tag{4.4}$$

$$p_{se} = {}_w p + \frac{a_f \cdot \sigma_{fy}}{{}_w t \cdot h_w \cdot {}_w\sigma_y} \tag{4.5}$$

$$\tan\theta = \sqrt{\left(\frac{h_w}{{}_W l + D}\right)^2 + 1} - \frac{h_w}{{}_W l + D} \tag{4.6}$$

where N_U: total axial force in the boundary columns (N); ${}_{sCS}A$, ${}_{mW}A$: cross section of the steel in the boundary column and the vertical reinforcement in the wall panel, respectively (mm^2); ${}_s\sigma_y$, ${}_W\sigma_y$: yield strengths of the steel in the boundary column and the vertical reinforcement in the wall panel, respectively (N/mm^2); l_w: distance between the centres of the boundary columns of the wall (mm); h_w: assumed height of applied lateral force (mm); ${}_Wt$: thickness of wall; ${}_Wl_t$: equivalent wall length of truss mechanism (=l); p_{se}: lateral reinforcement ratio; a_f: cross section of the steel flange in the boundary beam (mm^2); σ_{fy}: yield strength of the steel flange in the boundary beam; ϕ: angle of truss mechanism ($\cot\phi = 1$); θ: angle of arch mechanism; β: contribution ratio of the compressive concrete in the truss

Table 4.1 Calculated strength and maximum strength

Specimen			*CWAS*	*CWBS*	*CWAF*	*CWBF*
Maximum strength		Q_{exp} (kN)	1328	1336	971	1018
Flexural strength		Q_{mu} (kN)	1178	1266	786	844
Shear strength	Truss-Arch Eqn	Q_{su} (kN)	1319	1361	1202	1192
Ratio of maximum strength to calculated strength	Flexural strength	Q_{exp}/Q_{mu}	-	-	1.24	1.21
	Truss-Arch Eqn	Q_{exp}/Q_{su}	1.01	0.98	-	-

mechanism; v: effective factor for the compressive strength of concrete; ${}_c\sigma_B$: concrete strength (N/mm^2); ${}_wl_a$: equivalent wall length of arch mechanism; ${}_{CS}M_U$: ultimate flexural moment of the boundary column.

As for Specimens CWAS and CWBS with shear failure mode, the ratios of the maximum shear strength to the calculated by Truss-Arch Equation were about 1.0. Therefore, good agreements were obtained between the maximum strength and the calculated strength.

As for Specimens CWAF and CWBF with flexural failure mode, on the other hand, the ratios of the maximum strength to calculated flexural strength is about 1.2. Thus it is showed that the flexural strength of CES shear walls can be approximately estimated by Eqn. 4.1

5. CONCLUSIONS

In this study, cyclic loading tests of CES shear walls using a simplified longitudinal wall reinforcement arrangement were conducted. The failure mode, lateral load carrying capacity and deformation capacity of the CES shear walls were examined. The following conclusions can be drawn.

1) Regardless of failure mode, it was confirmed that the anchorage condition for the longitudinal wall reinforcement had little effect on the maximum strength of CES shear walls.

2) Specimen CWAS, without wall reinforcement anchorage, showed shear failure at the region of the upper corner of the first-story wall panel, while Specimen CWBS, which had wall reinforcement anchorage, showed shear failure across the first-story wall panel. It was found that the fracture region of the wall panel were different.

3) The deformation capacity of the CES shear walls improved by omitting the anchorage of the longitudinal wall reinforcement, because the damaged area of concrete of wall panel was reduced by the occurrence of slip between the wall panel and boundary beam after reaching the maximum strength.

4) It was confirmed that the ultimate flexural strength of the CES shear walls can be evaluated by the equation in the AIJ design standard for SRC structure, and that the ultimate shear strength of the CES shear walls can be evaluated using the Truss-Arch Equation.

References

Matsui, T. and Kuramoto, H. (2009). Static Loading Test on CES Columns with H-Shaped Steel under Different Axial Force Levels and Shear-Span Ratios. *Proceedings of the Eleventh Taiwan-Korea-Japan Joint Seminar on Earthquake Engineering for Building Structures* **25:2**, 289-294.

Nagata, S., Matsui, T. and Kuramoto, H. (2007). A Fundamental Study on Structural Performance of CES Beam-Column Joints. *Proceedings of the Japan Concrete Institute* **28:2**, 1279-1284.

Kuramoto, H., Matsui, T., Imamura, T. and Taguchi, T. (2007). Structural Performance of a Plane Frame for Composite CES Structural System. *Journal of Structural and Construction Engineering*, AIJ, **629**, 1103-1110

Haruyama, S., Onozato, N. and Tozawa, T. (2006). Study on Anchored Method of Reinforcing Bars Utilized for SRC Framed Shear Walls. Summaries of Technical Paper of Annual Meeting, AIJ, **C-1**, 1261-1264.

Architectural Institute of Japan (2001). AIJ Standards for Structural Calculation of Steel Reinforced Concrete Structures